PHYSICAL SCIENCES

The fate of carbon dioxide in water-rich fluids under extreme conditions

Ding Pan[1]* and Giulia Galli[1,2]

Investigating the fate of dissolved carbon dioxide under extreme conditions is critical to understanding the deep carbon cycle in Earth, a process that ultimately influences global climate change. We used first-principles molecular dynamics simulations to study carbonates and carbon dioxide dissolved in water at pressures (*P*) and temperatures (*T*) approximating the conditions of Earth's upper mantle. Contrary to popular geochemical models assuming that molecular CO_2(aq) is the major carbon species present in water under deep Earth conditions, we found that at 11 GPa and 1000 K, carbon exists almost entirely in the forms of solvated carbonate (CO_3^{2-}) and bicarbonate (HCO_3^-) ions and that even carbonic acid [H_2CO_3(aq)] is more abundant than CO_2(aq). Furthermore, our simulations revealed that ion pairing between Na^+ and CO_3^{2-}/HCO_3^- is greatly affected by *P-T* conditions, decreasing with increasing pressure at 800 to 1000 K. Our results suggest that in Earth's upper mantle, water-rich geofluids transport a majority of carbon in the form of rapidly interconverting CO_3^{2-} and HCO_3^- ions, not solvated CO_2(aq) molecules.

INTRODUCTION

The threat of global warming and climate change makes the understanding of Earth's carbon cycle a critical and pressing task. In Earth's lithosphere, sedimentary carbonates are considered to be the largest carbon hosts (*1*), with carbon transport between Earth's surface and interior (*2*) continuously occurring over millions to billions of years (*3*). For example, carbon belonging to organic matter and carbonate minerals may go deep into Earth's mantle within subduction zones, and it may be brought back to the surface by volcanism through CO_2 degassing (*4*). The deep carbon cycle substantially influences the carbon budget near Earth's surface, which, in turn, affects our energy consumption and global climate change (*4*). However, whether carbon accumulates in our planet's interior is still a subject of debate, and the chemical reactions leading to the predominant species of carbon in deep Earth are not yet well understood; hence, the means by which carbon transport occurs within Earth has not yet been established (*2*).

Carbon may be transported by crustal and mantle fluids in subduction zones (*5*), where water is a major transport medium (*6*). However, the forms of dissolved carbon in water under deep Earth conditions are poorly known. In Earth's upper mantle, the pressure (*P*) may reach ~13 GPa and the temperature (*T*) ~1700 K (*7*). It is challenging to study aqueous solutions of CO_2 and carbonates in the laboratory at these conditions, because water becomes highly corrosive (*8*, *9*) and it is difficult to obtain clear vibrational spectroscopic signals, which are commonly used to characterize aqueous solutions under ambient conditions. Additionally, the interpretation of existing Raman spectra measured at high *P-T* is controversial, because it is yet unclear how to relate the solute concentration to the observed signals under supercritical conditions (*10*, *11*). Experimental data have been obtained either at high *P* (HP) or at high *T* (HT), but it has not yet been possible to reach both HP and HT, as shown in Fig. 1. Therefore, our understanding of the chemistry of aqueous carbon is limited to *P-T* conditions of shallow mantle environments (*12*). Because of the lack of experimental data, traditional geochemical models have been based on several assumptions, one of which is that CO_2(aq) is the major dissolved carbon species in supercritical water under oxidizing conditions [for example, (*13*–*15*) and references therein].

Here, by conducting extensive first-principles molecular dynamics (MD) simulations, we studied Na_2CO_3 and CO_2 aqueous solutions at 11 GPa and 1000 K, that is, at pressures similar to those at the bottom of Earth's upper mantle. We note that ab initio simulations, which do not require any experimental input, have been shown to be powerful tools to study chemical reactions under extreme conditions (*16*). However, they are computationally demanding and cannot yet be used to carry out a detailed study of the whole *P-T* range in Earth's mantle. Instead, the present study focuses on general properties of dissolved carbon in water under extreme conditions; such conditions could not be addressed by simple models, which do not explicitly take into account the molecular nature of water and hence the way it dissociates under pressure. Contrary to the assumption that CO_2(aq) is the major carbon species under oxidizing conditions, we found that most of the dissolved carbon is in the form of CO_3^{2-} and HCO_3^-, with continuous transformation of the two species into each other on the scale of picoseconds. Surprisingly, even H_2CO_3(aq) is more abundant than CO_2(aq) when CO_2 is directly dissolved into water at 11 GPa and 1000 K. We also found that ion pairing occurs between Na^+ and CO_3^{2-} or HCO_3^-. Our study confirms that the molecular structure of supercritical water is markedly different from that of the liquid under ambient conditions and shows that the fast chemical dynamics in aqueous solutions under extreme conditions is key to understanding dissolved carbon in deep geofluids. Our findings suggest that at the bottom of the upper mantle, solvated CO_2(aq) is hardly present in water, with most of the species being carbonate and bicarbonate ions. We expect these highly active ionic species to be involved in the carbon recycling process in subduction zones in deep Earth and to play an important role in the transport of carbon.

RESULTS AND DISCUSSION

Validation of computational strategy

Before carrying out simulations at Earth's mantle conditions, we validated our computational strategy; in particular, we tested the accuracy of exchange-correlation (xc) functionals used in density functional theory by simulating a carbonate solution at 0.2 GPa and 823 K, for which experimental spectroscopic studies and geochemical models are available (*17*). We considered 1 Na_2CO_3 molecule and 62 water molecules (molality, 0.9 *m*) in a cubic simulation box with a side length of 14.42 Å. According to the equations of state by Zhang and Duan (*14*, *18*), which

[1]The Institute for Molecular Engineering, the University of Chicago, Chicago, IL 60637, USA. [2]Argonne National Laboratory, Argonne, IL 60439, USA.
*Corresponding author. Email: dingpan@uchicago.edu

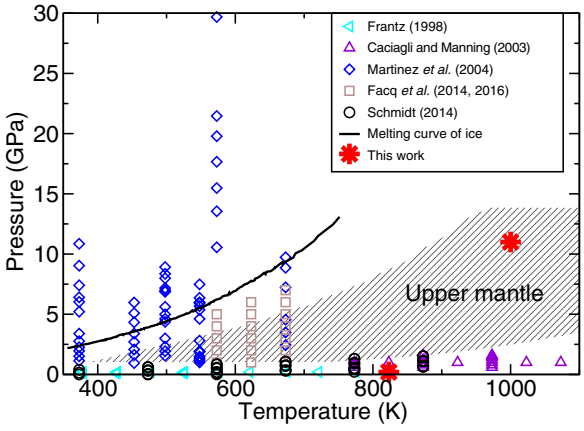

Fig. 1. High-pressure and high-temperature conditions reached in experiments on dissolved carbon in supercritical water, together with the conditions simulated in the present work: Frantz (*10*), Caciagli and Manning (*30*), Martinez *et al.* (*19*), Facq *et al.* (*31*, *36*), and Schmidt (*11*). The melting curve of ice is from the study by Datchi *et al.* (*51*). The shaded area shows the *P-T* conditions of the upper mantle (*7*).

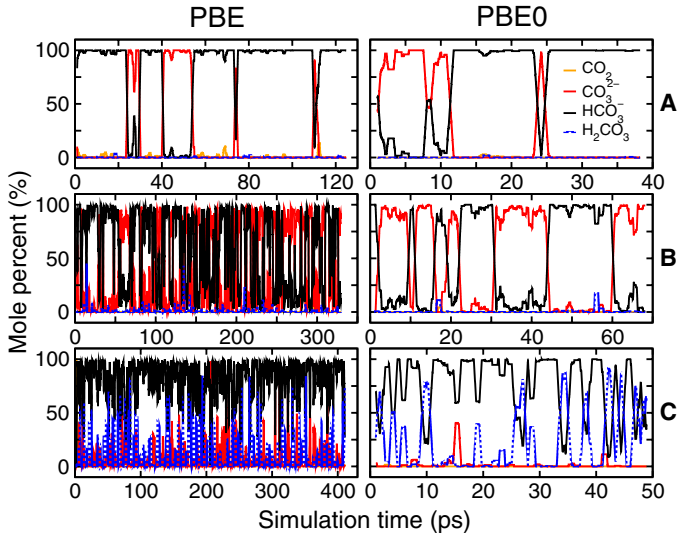

Fig. 2. Mole percents of CO_2 (orange), CO_3^{2-} (red), HCO_3^- (black), and H_2CO_3 (blue) as functions of simulation time in first-principles MD simulations. (**A**) Na_2CO_3 solution [0.9 *m* (molality)] at 0.2 GPa and 823 K. (**B**) Na_2CO_3 solution (0.9 *m*) at 11 GPa and 1000 K. (**C**) CO_2 solution (0.9 *m*) at 11 GPa and 1000 K. Calculations carried out with two xc functionals: PBE (*22*) and PBE0 (*23*) are compared.

are fitted to experimental data, the density of water under these conditions corresponds to a pressure of ~0.2 GPa. We chose sodium as a representative cation because Na_2CO_3 has a large solubility in supercritical water (*11*, *19*, *20*); Na is the seventh most abundant element in Earth's mantle (*21*).

Figure 2A shows the mole percents of CO_2(aq), CO_3^{2-}, HCO_3^-, and H_2CO_3(aq) species as functions of simulation time in first-principles MD simulations carried out with semilocal [PBE (Perdew-Burke-Ernzerhof) (*22*)] and hybrid [PBE0 (*23*)] functionals. The overall mole percents in our extensive MD simulations are summarized in Table 1. Using PBE, we found that bicarbonate is the dominating carbon species in the solution, with ~82% (mole percent of total dissolved carbon; see also Methods) bicarbonate ions and ~17% carbonate ions over a ~130-ps MD simulation. The amounts of CO_2(aq) and H_2CO_3(aq) were negligible. The lifetime of bicarbonate ions exceeded 10 ps in our simulations, whereas the lifetime of CO_3^{2-} was much shorter.

It is known that generalized gradient approximations (GGAs) may not be accurate in the description of solvated doubly-charged anions because of the charge delocalization error (*24*). For example, in sulfuric acid aqueous solutions under ambient conditions, Wan *et al.* found that the concentration of SO_4^{2-} was seriously overestimated when using the PBE functional, whereas the hybrid functional PBE0, which better describes the charge localization of solvated anions (*25*), gave results in qualitative agreement with experiments (*26*–*28*). Thus, we compared PBE and PBE0 simulations in order to extract robust trends from our results. We started a PBE0 simulation from a ~40-ps-long PBE simulation. As shown in Fig. 2A, HCO_3^- ions immediately transformed into CO_3^{2-} anions. In the subsequent simulation, the total mole percent of HCO_3^- was 27%, indicating that PBE overestimates the concentration of HCO_3^- with respect to PBE0. However, in both PBE and PBE0 simulations, we found that few CO_2(aq) or H_2CO_3(aq) molecules were present in the solution at 0.2 GPa and 823 K. Thus, the absence of these species in the solution was considered to be a robust result of our first-principles MD simulations.

Using experimental Raman spectroscopy (*10*), Frantz studied a 1 *m* K_2CO_3 solution under the same *P-T* conditions as those considered here. The concentration of a given species (C_i) was related to the measured Raman intensity (I_i) by $I_i = \gamma_i C_i$, where γ_i is the Raman scattering cross section. On the basis of the concentrations calculated by geochemical models, Frantz estimated that the ratio $\frac{\gamma_{carbonate}}{\gamma_{bicarbonate}}$ decreased by ~75% when increasing *T* from 523 to 823 K (*10*). Recently, after reexamining Frantz's spectroscopic data, Schmidt argued that this ratio should change by less than 10% in that temperature range (*11*), indicating that the species concentrations obtained by geochemical models in Frantz's study (*10*) may be questionable. Our theoretical concentrations are closer to the results obtained by the γ ratio proposed by Schmidt (*11*) than by Frantz (*10*). Using Schmidt's γ ratio and the published Raman spectra (*10*), we computed the mole percents of oxidized carbon in the solution and found 68% HCO_3^- and 32% CO_3^{2-} [no CO_2(aq)-related Raman peaks were reported in Frantz's study]. Therefore, PBE appears to overestimate the amount of HCO_3^- by ~20% relative to the value obtained from Frantz's spectroscopic data (*10*) and the γ ratio proposed by Schmidt (*11*); however, the overestimate is not as serious as for sulfuric acid aqueous solutions under ambient conditions, for example (*26*). This finding is consistent with our previous investigation of water under pressure, where we found that PBE performs better under extreme conditions than under ambient conditions in terms of equation of state of water, as well as in predicting static and electronic dielectric constants (*20*, *29*). On the other hand, our PBE0 simulations yield results much closer to the experimental data. Our validation strategy led us to conclude that the use of the PBE functional is justified at high *P* and *T*, where some additional PBE0 simulations were carried out to double-check our PBE results.

Absence of CO_2(aq)

The simulations described above led us to question the assumption of CO_2(aq) being the major carbon species in supercritical aqueous fluids in deep Earth. We further increased the pressure to ~11 GPa and the temperature to 1000 K, that is, pressures similar to those at the bottom of Earth's upper mantle, to investigate whether our conclusions

Table 1. Carbon species in the 0.9 *m* Na_2CO_3 and 0.9 *m* CO_2 solutions in first-principles MD simulations. The concentrations are shown as mole percents of the total dissolved carbon. The mole percents of CO_3^{2-} and HCO_3^- include those of ion pairs formed by them, respectively. The experimental results (Expt.) are from the Raman data in the study by Frantz (*10*) (see text). N/A, not applicable.

Solution	*P* (GPa)	*T* (K)	Method	Carbon species (%)			
				CO_2	CO_3^{2-}	HCO_3^-	H_2CO_3
Na_2CO_3	0.2	823	PBE	0.6	16.7	82.4	0.1
			PBE0	0.2	26.8	72.9	0.1
			Expt.	N/A	32	68	N/A
	11	1000	PBE	0.1	40.8	57.9	1.2
			PBE0	0.1	51.8	47.5	0.6
CO_2	11	1000	PBE	0.6	8.2	79.8	11.4
			PBE0	0.0	1.7	75.0	23.3

on the absence of CO_2(aq) in water did hold under more extreme conditions. The density of water at this *P*-*T* condition is 1.57 g/cm^3 (*20*). The equation of state of water in this regime has been investigated in our previous study with the PBE functional (*20*).

Figure 2B shows the mole percents of dissolved carbon species as functions of simulation time obtained in first-principles MD simulations with the PBE and PBE0 functionals. We found 41% CO_3^{2-}, 58% HCO_3^-, and 1% H_2CO_3(aq) when using PBE; PBE0 simulations gave 52% CO_3^{2-} and 48% HCO_3^-, as shown in Table 1. Similar to our finding at 0.2 GPa and 823 K, PBE yields a higher concentration of HCO_3^- than PBE0, but the results of the two simulations are closer than at lower *P* and *T*. Less than 1% CO_2(aq) was found in both PBE and PBE0 simulations.

Because of the lack of experimental data, many studies under the upper mantle conditions used geochemical models based on extrapolations of available data. Using extrapolated thermodynamic data, Caciagli and Manning considered CO_2(aq) as the dominant dissolved carbon species in aqueous calcite solutions up to 1.6 GPa and 1023 K (*30*). On the basis of geochemical models at lower *P* and *T*, Manning *et al.* inferred that bicarbonate ions would become less favored relative to CO_2(aq) under the mantle conditions (*12*). However, Facq *et al.* performed Raman studies of $CaCO_3$ solutions up to 7 GPa and 673 K and found that at $P > 4$ GPa, CO_3^{2-} is the dominant carbon species (*31*). Furthermore, on the basis of theoretical models, Facq *et al.* speculated that at higher temperature, CO_2(aq) may become a dominant species, depending on the pressure, though no exact temperature or pressure was reported (*31*). In the studies by Caciagli and Manning (*30*) and Facq *et al.* (*31*), using solutions at equilibrium with $CaCO_3$ crystals, the concentrations of dissolved carbon were lower than those studied in this work; it is therefore challenging to experimentally detect the amount of CO_2(aq) and definitely rule out the existence of molecular CO_2. Our first-principles MD simulations clearly showed that up to 11 GPa and 1000 K, few CO_3^{2-} ions are converted to CO_2(aq).

To further verify whether CO_2(aq) may be stable in water under extreme conditions, we directly dissolved CO_2 into water under the same *P*-*T* condition of the simulation previously described (the carbonate ion was replaced by one CO_2 molecule and one water molecule in the same simulation box at ~11 GPa and 1000 K) and found again that only a low percentage of CO_2(aq) remained after the solution was equilibrated. Bicarbonate ions accounted for approximately 80% of dissolved carbon; this result was obtained using both xc functionals, as shown in Fig. 2C and Table 1.

We also found that H_2CO_3(aq) was present in the solution with a mole percent between 11 and 23%, depending on the functionals; note that this concentration is about 20 times larger than that of CO_2(aq), as shown in Table 1. The formation of H_2CO_3(aq) via CO_2(aq) hydration may follow one of two pathways (*32*): (i) CO_2(aq) directly reacts with a water molecule to generate H_2CO_3(aq) or (ii) an intermediate HCO_3^- is formed before H_2CO_3(aq). At 11 GPa and 1000 K, in both PBE and PBE0 simulations, we found that HCO_3^- formed first, followed by H_2CO_3(aq); however, frequent proton hopping events were detected between H_2CO_3(aq) and water. The lifetime of H_2CO_3(aq) is on the subpicosecond scale. The existence of H_2CO_3 was also found in a 55.5 *m* CO_2 water solution at ~32 GPa and 2000 K using first-principles MD with the GGA functional, but no concentration was given because the simulation was only 10 ps long (*33*).

In aqueous solutions under ambient conditions, H_2CO_3(aq) exists only in a very low concentration and rapidly reverts to CO_2(aq) and water (*12*)

$$H_2CO_3(aq) \rightarrow CO_2(aq) + H_2O \quad (1)$$

Because it is difficult to detect H_2CO_3(aq) at ambient conditions, current geochemical models cannot distinguish between H_2CO_3(aq) and CO_2(aq), and H_2CO_3(aq) and CO_2(aq) are modeled as the same species (*12*). However, our findings point out that this conventional treatment may ignore the important presence of H_2CO_3(aq) as a neutral carbon species in deep Earth.

Under ambient conditions, the dissociation reaction of CO_2(aq) in pure water

$$CO_2(aq) + 2H_2O \rightarrow HCO_3^- + H_3O^+ \quad (2)$$

is rather slow, with an activation free energy of 21.7 kcal/mol (0.94 eV) (*32*, *34*); more than 99% of CO_2 molecules remain intact when the concentration of CO_2(aq) is above 0.1 *m*. However, when the hydroxide ion (OH^-) is present, the activation free energy of the dissociation of CO_2(aq) is reduced to 12.0 kcal/mol (0.52 eV). As a result, the dissociation reaction is accelerated markedly; it is about 10^7 faster than that in pure water (*34*). Under HP-HT conditions, water molecules are more easily dissociated, producing hydroxide ions, which then react with hydrated CO_2(aq), thus enhancing its dissociation. The enhanced bending motion of C–O bonds at high *P*-*T* also facilitates the change of carbon hybridization from sp to sp^2. In our simulations, the exact concentrations of charged ions depend on the xc functionals used, but both the GGA and hybrid functionals give the same result on CO_2(aq) concentration: The latter is negligible in aqueous solutions at 11 GPa and 1000 K. Hence, we conclude that our calculations provide strong and robust evidence of the absence of CO_2(aq) in water under this *P*-*T* condition.

Ion pairing

Another important question regarding the aqueous solutions studied here concerns the interactions between (bi)carbonate ions and metal ions. In Fig. 3, we plot the radial distribution functions (RDFs) and distributions of the C–Na distances obtained from our MD trajectories using the PBE and PBE0 functionals. We first discuss the results given by the two functionals, and we then extract robust features of both simulations.

We examined the solution structures of (bi)carbonate ions in the solutions. In Fig. 3A, the C–O_w RDFs (where O_w denotes an O belonging to water molecules) obtained by PBE and PBE0 are very similar at 0.2 GPa, 823 K or 11 GPa, 1000 K. At 11 GPa and 1000 K, the first local minimum of the C–O_w RDFs is at ~4.54 Å, corresponding to the separation of the first and second solvation shells of (bi)carbonate ions. Although this minimum is not easily defined at 0.2 GPa and 823 K (because the first peak of the C–O_w RDFs also appears to vanish at ~4.54 Å), we used the same radial cutoff of 4.54 Å for the first solvation shells of (bi)carbonate ions under two *P-T* conditions to have a consistent comparison.

The ion pairing strength in an aqueous solution greatly depends on the static dielectric constant of water, ε_0: the electrostatic interaction between ions in water is $\frac{q_1 q_1}{\varepsilon_0 r^2}$, where q_1 and q_2 are the electrical charges of the ions, and r is the distance between them. We note that PBE appears to overestimate ε_0 under ambient conditions, whereas PBE0 yields a result in better agreement with experiment (*35*); hence, at the PBE level of theory, the overestimate of electrostatic screening leads to weaker ion pairing, as shown by lower PBE peaks at ~3.2 Å in Fig. 3B. Interestingly, under upper mantle pressure conditions, the discrepancy between ε_0 evaluated within PBE and the experimental value is rather small (*20*), and we expect PBE to yield more realistic ion associations under those conditions than at ambient conditions.

At 0.2 GPa and 823 K, both functionals show marked peaks in the distribution of the C–Na distance at ~3.2 Å, indicating strong ion pairing between Na^+ and CO_3^{2-} or HCO_3^-. The first peak of the C–O_w RDF is at ~3.5 Å, so the Na^+-CO_3^{2-}/HCO_3^- pairs tend to reside inside the first solvation shell of (bi)carbonate ions. With increasing *P* and *T* to 11 GPa and 1000 K, respectively, the main peak of the distribution function of the C–Na distance decreases in intensity, indicating that ion pairing becomes weaker in denser water.

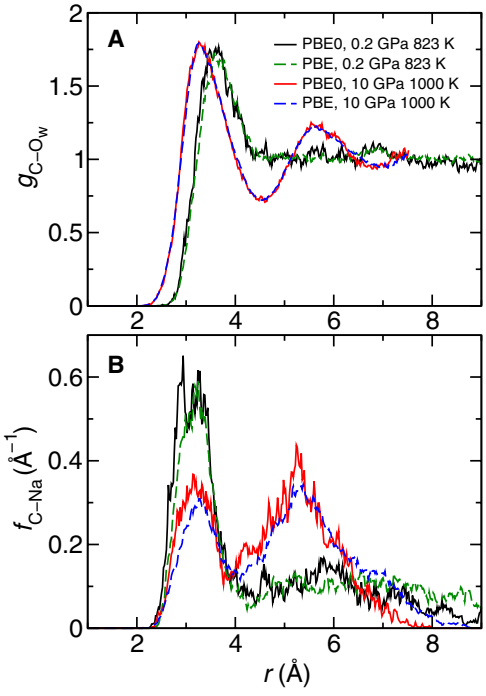

Fig. 3. The solvation structures of carbon species and ion pairing distances in the 0.9 *m* Na_2CO_3 solutions. (**A**) RDFs of carbon atoms (C) versus oxygen atoms of water (O_w). (**B**) Probability distributions of the distances between carbon atoms and sodium ions. The MD simulations on the 0.9 *m* Na_2CO_3 solutions were conducted at 0.2 GPa, 823 K and 11 GPa, 1000 K. Two xc functionals were compared: PBE and PBE0.

Table 2 shows the mole percents of the ion pairs in the first solvation shells of (bi)carbonate ions. As shown in Tables 1 and 2, we found that more than 99% of the CO_3^{2-} anions were accompanied by one or two Na^+ cations in their first solvation shells at 0.2 GPa and 823 K, whereas at 11 GPa and 1000 K, less than 63% of the CO_3^{2-} ions had counterions in the first solvation shells. This may be attributed to the change of ε_0: Our previous study showed that with increasing pressure, ε_0 increases along an isotherm (*20*), and thus, the dielectric screening is enhanced and the electrostatic attraction between Na^+ and CO_3^{2-} or HCO_3^- is weakened. The large dielectric screening also enhances the autoionization of water, producing a higher concentration of OH^- ions, whose presence accelerates the dissociation of CO_2.

The pairing of carbonate ions with alkali cations at 0.2 GPa and 823 K was also reported in a 1 *m* K_2CO_3 solution by using geochemical models (*10*), but no spectroscopic evidence was available because of the detection limit (*10*). Recently, Schmidt reported the Raman spectra, which were interpreted as showing Na^+-CO_3^{2-} pairing, for a 1.6 *m* Na_2CO_3 solution interfaced with quartz at *T* above 673 K. In the $CaCO_3$-water-NaCl solutions, Facq *et al.* interpreted the measured Raman data by assuming the existence of the $NaHCO_3^\circ$ complex (*36*). In our study, despite the different ion pairing strengths given by the two functionals, we found that ion pairing between Na^+ and CO_3^{2-} or HCO_3^- occurs at 0.2 GPa and 823 K, with its strength decreasing at 11 GPa and 1000 K.

Kinetics of reactions involving CO_3^{2-} and HCO_3^-

Bicarbonate and carbonate ions are the major species in the solutions studied here, with frequent proton transfer over picosecond time scales. Their chemical balance in the Na_2CO_3 solution is

$$CO_3^{2-} + H_2O \rightleftharpoons HCO_3^- + OH^- \quad (3)$$

The kinetics of the reaction is key to understanding the chemistry of oxidized carbon in supercritical water.

Figure 4 shows the distribution of protons hopping between a carbonate ion and its nearest water molecule in the Na_2CO_3 solution at 11 GPa and 1000 K. From Fig. 4, we calculated the effective free energy barrier of proton transfer to the right in reaction (3) as $\Delta F = -k_B T \ln \frac{P_b}{P_r}$, where P_b and P_r are the probabilities of being on the top of the barrier and in the reactant state, respectively, and k_B is the Boltzmann constant. At the PBE0 level of theory, the free energy barrier is estimated to be 4.6 kcal/mol

Table 2. The ion pairing in the first solvation shells of the carbon species in the 0.9 *m* Na_2CO_3 solutions. The concentrations are shown as mole percents of the total dissolved carbon.

P (GPa)	*T* (K)	Method	Ion pairing species (%)			
			$NaCO_3^-$	$Na_2CO_3^\circ$	$NaHCO_3^\circ$	$Na_2HCO_3^+$
0.2	823	PBE	3.7	13.0	59.7	7.5
		PBE0	8.4	18.2	40.8	18.2
11	1000	PBE	18.1	5.9	28.9	7.5
		PBE0	22.4	10.0	20.4	12.5

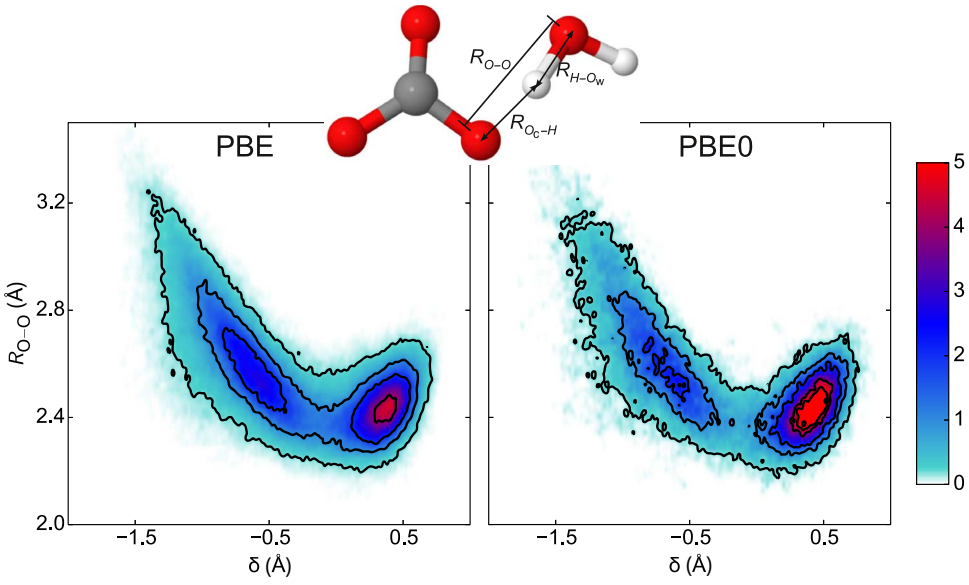

Fig. 4. Probability distributions of positions of protons hopping between CO_3^{2-} and H_2O in the Na_2CO_3 solution at 11 GPa and 1000 K. The unit is $Å^{-2}$. The reaction coordinate R_{O-O} is the distance between the two neighboring oxygen atoms, O_c and O_w, in carbonate ions and water molecules, respectively, and δ is the proton displacement $R_{O_c-H} - R_{H-O_w}$. Two xc functionals were compared: PBE and PBE0.

(0.20 eV), whereas at the PBE level, it decreases to ~2.8 kcal/mol (0.12 eV). According to the Arrhenius equation, the rate constant is Ae^{-E_a/k_BT}, where E_a is the activation energy. If we assume that PBE and PBE0 yield a similar prefactor A and approximate the activation energy by the free energy barrier, the rate constant of forward reaction (3) using PBE is about three times as large as that found using PBE0. This difference may be explained by the difference in O–H bond strengths obtained using the two functionals. We computed the vibrational density of states of the solution at 11 GPa and 1000 K in fig. S1 and found that the stretching frequency of O–H bonds given by PBE is about 150 cm^{-1} lower than that obtained with PBE0. As a result, at the PBE level of theory, the O–H bond is weaker and easier to break than at the PBE0 level, and the proton transfer rate is enhanced. It has been reported that at ambient conditions, the vibrational frequencies of the OH stretching mode are also underestimated using PBE compared with experimental data, whereas PBE0 yields results much closer to experiment (*37*). The underestimate decreases with increasing temperature (*37*). These findings suggest that it is necessary to use hybrid functionals to get accurate reaction rates in aqueous solutions, especially under ambient conditions. Under extreme conditions, the error of PBE becomes smaller, which is again consistent with the results of our previous studies (*20*, *29*).

At T = 1000 K, the thermal energy k_BT is 2.0 kcal/mol (0.086 eV), comparable to the free energy barriers given by PBE and PBE0. Because of the low free energy barrier and enhanced thermal effects, both functionals yield a rate constant of forward reaction (3) about six orders of magnitude faster than that at ambient conditions [the rate constant of forward reaction (3) is 3.06×10^5 s^{-1} in seawater under ambient conditions (*38*)], indicating highly active ionic interactions in our solutions at 11 GPa and 1000 K.

It is worth noting that Fig. 4 shows only part of reaction (3); the proton transfer not only is limited to the distance between a carbonate ion and a neighboring water molecule but also may involve multiple water molecules connected by a hydrogen bond (HB) wire, via a Grotthuss mechanism (*39*, *40*). In our solutions, protons move back and forth along HB wires over short time scales (<0.1 ps), leading to short-lived (bi)carbonate ions. However, if the thermal fluctuation breaks HB wires, protons cannot hop back and then bicarbonate ions persist for a few picoseconds. The forming and breaking of the HB wires are critical to the lifetime of carbon species in the calculations reported here.

In Raman experiments, the symmetric stretching mode of C–O/C–OH at ~1000 cm^{-1} is used to detect carbonate or bicarbonate ions. The vibrational period of this mode is 33 fs. For the carbon species, whose lifetime is comparable to 33 fs or even shorter, the Raman peaks are broadened considerably and may be difficult to identify experimentally.

In our MD simulations, the forces acting on nuclei were computed quantum mechanically, but protons were still treated as classical particles. If quantum nuclear effects are taken into account, we expect the proton transfer rate to be enhanced, though at such high temperatures, quantum effects may not be as important as under ambient conditions (*41*).

With both PBE and PBE0 functionals, van der Waals interactions are described inaccurately; however, in our study, we focused on the breaking and forming of covalent bonds, and the lack of dispersion forces is not expected to affect our main conclusions. In addition, we note that the results for the equilibrium volume and dielectric constant of ice obtained with PBE and van der Waals functionals agree much better at high pressure (for example, for ice VIII) than at low pressure (for example, for ice Ih and Ic) (*42*, *43*), indicating that the lack of dispersion forces may affect the results for water and ice more under ambient conditions than under pressure.

Widely used geochemical models based on the Born function, for example, the Helgeson-Kirkham-Flowers model as implemented in SUPCRT92 (*17*), consider water as a continuum medium with no molecular structure taken into account, when calculating thermodynamic properties of electrolytes (*44*). In our study, we found that the microscopic properties of water at the molecular scale, for example, proton transfer mechanisms, play a substantial role in the chemical reactions of oxidized carbon, particularly under the high P-T conditions studied here.

CONCLUSION

In conclusion, we carried out first-principles MD simulations to investigate dissolved carbonate and CO_2 in water at high pressure and high temperature, up to the conditions of Earth's upper mantle. Contrary to popular geochemical models assuming that CO_2(aq) is the major carbon species present in water, we found that most of the dissolved carbon at 11 GPa and 1000 K is in the form of solvated CO_3^{2-} and HCO_3^- anions. The two anions exchange protons with water on a picosecond time scale. The proton transfer along hydrogen bond wires driven by thermal fluctuations is responsible for the fast dynamics observed in these solutions. Under these extreme conditions, even H_2CO_3(aq) is more abundant than CO_2(aq), a marked difference with respect to ambient conditions. Although it is well known that the autoionization of water is greatly enhanced under extreme conditions, for example, under the *P-T* conditions of Earth's mantle, and that the pH of neutral water may be well below 7 (*6*), it has been long unclear how the notable properties of water under pressure affect the solvation of oxidized carbon. Using atomistic ab initio simulations, we showed that the coordination number of carbon changes in water under Earth's upper mantle conditions. We also found that ion pairing between Na^+ and CO_3^{2-} or HCO_3^- is greatly affected by *P-T* conditions, decreasing with pressure at 800 to 1000 K. Our results suggest that under extreme conditions, water transports carbon mostly through highly active ions, not CO_2(aq) molecules.

The results reported here give important insights into deep carbon science. Our calculations predicted that the carbon dissolved in water-rich geofluids is in ionic forms in the bottom of Earth's upper mantle, indicating that CO_2 degassing may mostly occur close to Earth's surface.

METHODS

First-principles MD simulations were performed in the Born-Oppenheimer approximation using the Qbox code (http://qboxcode.org/) (*45*). Two xc functionals were used: the semilocal functional PBE and the hybrid functional PBE0. To improve the efficiency of our calculations using PBE0, the recursive subspace bisection method was used with a threshold of 0.02 (*46*, *47*). The Brillouin zone of the supercell was sampled with the Γ point only. We used norm-conserving pseudopotentials (Pseudopotential Table, http://fpmd.ucdavis.edu/potentials) (*48*, *49*) with a kinetic cutoff of 85 Ry, which was increased to 220 Ry for pressure calculations. The MD time step was 0.24 fs. Deuterium was used instead of hydrogen, so as to use a larger time step for computational convenience. Note that the density given in the main text was computed for light water. The temperature was maintained constant by the Bussi-Donadio-Parrinello thermostat (τ = 24.2 fs) (*50*).

To determine whether CO_2 or CO_3^{2-} was present in our simulations, we searched the atomic trajectories generated in our simulations for the three closest O atoms to a given C atom and ordered these O atoms according to their respective C–O distances. If the C–O distance of the third closest O atom was larger than that of the second one by more than 0.4 Å, the species was considered to be CO_2; otherwise, it was defined as a CO_3^{2-} anion. The C–O bond length in all sets of our MD runs was found to be 1.3 ± 0.2 Å. For H atoms around the carbonate ion, we sought the nearest O atom to each H atom, and if this O atom belonged to the carbonate ion, we concluded that a bicarbonate ion, HCO_3^-, was formed. When two H atoms were bonded to CO_3^{2-} simultaneously, the solute then became carbonic acid.

Using the criteria described above, we determined the type of solute molecules present in our MD simulations at each time step. Note that under HP-HT conditions, covalent bonds are frequently broken and reformed; hence, to establish how the concentration of the solute varied along our MD trajectories, we calculated the mole percents of carbon species as functions of simulation time. The mole percent of the *i*th species at time *t* was obtained as

$$x_i(t) = \frac{n_i(t)}{N_w} \times 100\% \quad (4)$$

where $n_i(t)$ is the number of the snapshots containing the *i*th species between the time $(t - \tau_w)$ and *t*, and N_w is the total number of snapshots in this time interval. Here, τ_w was set to 1 ps.

SUPPLEMENTARY MATERIALS

Supplementary material for this article is available at http://advances.sciencemag.org/cgi/content/full/2/10/e1601278/DC1

fig. S1. The vibrational density of states of the 0.9 *m* Na_2CO_3 solution at ~11 GPa and 1000 K.
fig. S2. Probability distributions of positions of protons hopping between CO_3^{2-} and H_2O in the Na_2CO_3 solution at 0.2 GPa and 823 K.

REFERENCES AND NOTES

1. P. Falkowski, R. J. Scholes, E. Boyle, J. Canadell, D. Canfield, J. Elser, N. Gruber, K. Hibbard, P. Högberg, S. Linder, F. T. Mackenzie, B. Moore III, T. Pedersen, Y. Rosenthal, S. Seitzinger, V. Smetacek, W. Steffen, The global carbon cycle: A test of our knowledge of Earth as a system. *Science* **290**, 291–296 (2000).
2. C. E. Manning, Geochemistry: A piece of the deep carbon puzzle. *Nat. Geosci.* **7**, 333–334 (2014).
3. D. J. DePaolo, Sustainable carbon emissions: The geologic perspective. *MRS Energy Sustainability* **2**, E9 (2015).
4. R. Dasgupta, M. M. Hirschmann, The deep carbon cycle and melting in Earth's interior. *Earth Planet. Sci. Lett.* **298**, 1–13 (2010).
5. P. B. Kelemen, C. E. Manning, Reevaluating carbon fluxes in subduction zones, what goes down, mostly comes up. *Proc. Natl. Acad. Sci. U.S.A.* **112**, E3997–E4006 (2015).
6. A. Liebscher, Aqueous fluids at elevated pressure and temperature. *Geofluids* **10**, 3–19 (2010).
7. A. B. Thompson, Water in the Earth's upper mantle. *Nature* **358**, 295–302 (1992).
8. H. Weingärtner, E. U. Franck, Supercritical water as a solvent. *Angew. Chem. Int. Ed.* **44**, 2672–2692 (2005).
9. J.-F. Lin, E. Gregoryanz, V. V. Struzhkin, M. Somayazulu, H.-k. Mao, R. J. Hemley, Melting behavior of H_2O at high pressures and temperatures. *Geophys. Res. Lett.* **32**, L11306 (2005).
10. J. D. Frantz, Raman spectra of potassium carbonate and bicarbonate aqueous fluids at elevated temperatures and pressures: Comparison with theoretical simulations. *Chem. Geol.* **152**, 211–225 (1998).
11. C. Schmidt, Raman spectroscopic determination of carbon speciation and quartz solubility in H_2O+Na_2CO_3 and H_2O+$NaHCO_3$ fluids to 600 °C and 1.53 GPa. *Geochim. Cosmochim. Acta* **145**, 281–296 (2014).
12. C. E. Manning, E. L. Shock, D. Sverjensky, The chemistry of carbon in aqueous fluids at crustal and upper mantle conditions: Experimental and theoretical constraints. *Rev. Mineral Geochem.* **75**, 109–148 (2013).
13. Z. Duan, Z. Zhang, Equation of state of the H_2O, CO_2, and H_2O–CO_2 systems up to 10 GPa and 2573.15 K: Molecular dynamics simulations with ab initio potential surface. *Geochim. Cosmochim. Acta* **70**, 2311–2324 (2006).
14. C. Zhang, Z. Duan, A model for C-O-H fluid in the Earth's mantle. *Geochim. Cosmochim. Acta* **73**, 2089–2102 (2009).
15. J.-M. Huizenga, Thermodynamic modelling of C–O–H fluids. *Lithos* **55**, 101–114 (2001).
16. F. Gygi, G. Galli, Ab initio simulation in extreme conditions. *Mater. Today* **8**, 26–32 (2005).
17. J. W. Johnson, E. H. Oelkers, H. C. Helgeson, SUPCRT92: A software package for calculating the standard molal thermodynamic properties of minerals, gases, aqueous species, and reactions from 1 to 5000 bar and 0 to 1000 degC. *Comput. Geosci.* **18**, 899–947 (1992).
18. Z. Zhang, Z. Duan, Prediction of the *PVT* properties of water over wide range of temperatures and pressures from molecular dynamics simulation. *Phys. Earth Planet Inter.* **149**, 335–354 (2005).
19. I. Martinez, C. Sanchez-Valle, I. Daniel, B. Reynard, High-pressure and high-temperature Raman spectroscopy of carbonate ions in aqueous solution. *Chem. Geol.* **207**, 47–58 (2004).

20. D. Pan, L. Spanu, B. Harrison, D. A. Sverjensky, G. Galli, Dielectric properties of water under extreme conditions and transport of carbonates in the deep Earth. *Proc. Natl. Acad. Sci. U.S.A.* **110**, 6646–6650 (2013).
21. I. Jackson, *The Earth's Mantle: Composition, Structure, and Evolution* (Cambridge Univ. Press, 2000).
22. J. P. Perdew, K. Burke, M. Ernzerhof, Generalized gradient approximation made simple. *Phys. Rev. Lett.* **77**, 3865–3868 (1996).
23. C. Adamo, V. Barone, Toward reliable density functional methods without adjustable parameters: The PBE0 model. *J. Chem. Phys.* **110**, 6158–6170 (1999).
24. A. J. Cohen, P. Mori-Sánchez, W. Yang, Insights into current limitations of density functional theory. *Science* **321**, 792–794 (2008).
25. A. P. Gaiduk, C. Zhang, F. Gygi, G. Galli, Structural and electronic properties of aqueous NaCl solutions from ab initio molecular dynamics simulations with hybrid density functionals. *Chem. Phys. Lett.* **604**, 89–96 (2014).
26. Q. Wan, L. Spanu, F. Gygi, G. Galli, Electronic structure of aqueous sulfuric acid from first-principles simulations with hybrid functionals. *J. Phys. Chem. Lett.* **5**, 2562–2567 (2014).
27. M. Guidon, F. Schiffmann, J. Hutter, J. VandeVondele, Ab initio molecular dynamics using hybrid density functionals. *J. Chem. Phys.* **128**, 214104 (2008).
28. R. A. DiStasio Jr., B. Santra, Z. Li, X. Wu, R. Car, The individual and collective effects of exact exchange and dispersion interactions on the ab initio structure of liquid water. *J. Chem. Phys.* **141**, 084502 (2014).
29. D. Pan, Q. Wan, G. Galli, The refractive index and electronic gap of water and ice increase with increasing pressure. *Nat. Commun.* **5**, 3919 (2014).
30. N. C. Caciagli, C. E. Manning, The solubility of calcite in water at 6–16 kbar and 500–800 ° C. *Contrib. Mineral. Petrol.* **146**, 275–285 (2003).
31. S. Facq, I. Daniel, G. Montagnac, H. Cardon, D. A. Sverjensky, In situ Raman study and thermodynamic model of aqueous carbonate speciation in equilibrium with aragonite under subduction zone conditions. *Geochim. Cosmochim. Acta* **132**, 375–390 (2014).
32. A. Stirling, I. Pápai, H_2CO_3 forms via HCO_3^- in water. *J. Phys. Chem. B* **114**, 16854–16859 (2010).
33. J.-B. Maillet, E. Bourasseau, Ab initio simulations of thermodynamic and chemical properties of detonation product mixtures. *J. Chem. Phys.* **131**, 084107 (2009).
34. X. Wang, W. Conway, R. Burns, N. McCann, M. Maeder, Comprehensive study of the hydration and dehydration reactions of carbon dioxide in aqueous solution. *J. Phys. Chem. A* **114**, 1734–1740 (2009).
35. M. Schönherr, B. Slater, J. Hutter, J. VandeVondele, Dielectric properties of water ice, the ice Ih/XI phase transition, and an assessment of density functional theory. *J. Phys. Chem. B* **118**, 590–596 (2014).
36. S. Facq, I. Daniel, G. Montagnac, H. Cardon, D. A. Sverjensky, Carbon speciation in saline solutions in equilibrium with aragonite at high pressure. *Chem. Geol.* **431**, 44–53 (2016).
37. C. Zhang, D. Donadio, F. Gygi, G. Galli, First principles simulations of the infrared spectrum of liquid water using hybrid density functionals. *J. Chem. Theory Comput.* **7**, 1443–1449 (2011).
38. K. G. Schulz, U. Riebesell, B. Rost, S. Thoms, R. E. Zeebe, Determination of the rate constants for the carbon dioxide to bicarbonate inter-conversion in pH-buffered seawater systems. *Mar. Chem.* **100**, 53–65 (2006).
39. D. Marx, Proton transfer 200 years after von Grotthuss: Insights from ab initio simulations. *Chemphyschem* **7**, 1848–1870 (2006).
40. P. L. Geissler, C. Dellago, D. Chandler, J. Hutter, M. Parrinello, Autoionization in liquid water. *Science* **291**, 2121–2124 (2001).
41. M. Ceriotti, J. Cuny, M. Parrinello, D. E. Manolopoulos, Nuclear quantum effects and hydrogen bond fluctuations in water. *Proc. Natl. Acad. Sci. U.S.A.* **110**, 15591–15596 (2013).
42. B. Santra, J. Klimeš, D. Alfè, A. Tkatchenko, B. Slater, A. Michaelides, R. Car, M. Scheffler, Hydrogen bonds and van der Waals forces in ice at ambient and high pressures. *Phys. Rev. Lett.* **107**, 185701 (2011).
43. É. D. Murray, G. Galli, Dispersion interactions and vibrational effects in ice as a function of pressure: A first principles study. *Phys. Rev. Lett.* **108**, 105502 (2012).
44. G. M. Anderson, *Thermodynamics of Natural Systems* (Cambridge Univ. Press, ed. 2, 2005).
45. F. Gygi, Architecture of Qbox: A scalable first-principles molecular dynamics code. *IBM J. Res. Dev.* **52**, 137–144 (2008).
46. F. Gygi, Compact representations of Kohn-Sham invariant subspaces. *Phys. Rev. Lett.* **102**, 166406 (2009).
47. F. Gygi, I. Duchemin, Efficient computation of Hartree–Fock exchange using recursive subspace bisection. *J. Chem. Theory Comput.* **9**, 582–587 (2012).
48. D. R. Hamann, M. Schlüter, C. Chiang, Norm-conserving pseudopotentials. *Phys. Rev. Lett.* **43**, 1494–1497 (1979).
49. D. Vanderbilt, Optimally smooth norm-conserving pseudopotentials. *Phys. Rev. B Condens. Matter* **32**, 8412–8415 (1985).
50. G. Bussi, D. Donadio, M. Parrinello, Canonical sampling through velocity rescaling. *J. Chem. Phys.* **126**, 014101 (2007).
51. F. Datchi, P. Loubeyre, R. LeToullec, Extended and accurate determination of the melting curves of argon, helium, ice (H_2O), and hydrogen (H_2). *Phys. Rev. B* **61**, 6535–6546 (2000).

Acknowledgments: We thank F. Giberti and D. Gygi for many useful discussions and D. A. Sverjensky for the critical reading of the manuscript and many discussions. **Funding:** This work was supported by the Alfred P. Sloan Foundation through the Deep Carbon Observatory (DCO) and by U.S. Department of Energy (DOE)–Basic Energy Sciences grant no. DE-SC0008938. Part of this work was carried out using the DCO Computer Cluster and resources of the Argonne Leadership Computing Facility (ALCF), provided by an award of computer time by the Innovative and Novel Computational Impact on Theory and Experiment (INCITE) program. ALCF is a DOE Office of Science User Facility supported under contract DE-AC02-06CH11357. We also acknowledge the University of Chicago Research Computing Center for support of this work. **Author contributions:** D.P. and G.G. designed the research. Calculations were performed by D.P. All authors contributed to the analysis and discussion of the data and the writing of the manuscript. **Competing interests:** The authors declare that they have no competing interests. **Data and materials availability:** All data needed to evaluate the conclusions in the paper are present in the paper and/or the Supplementary Materials. Additional data related to this paper may be requested from the authors.

Submitted 7 June 2016
Accepted 2 September 2016
Published 12 October 2016
10.1126/sciadv.1601278

Citation: D. Pan, G. Galli, The fate of carbon dioxide in water-rich fluids under extreme conditions. *Sci. Adv.* **2**, e1601278 (2016).